Inhalation Toxicology, 15:553–587, 2003

0895–8378/03 $12.00 + .00
DOI: 10.1080/08958370390205074

Taylor & Francis
healthsciences

MODELING THE RETENTION AND CLEARANCE OF MANMADE VITREOUS FIBERS IN THE RAT LUNG

C. L. Tran, A. D. Jones, B. G. Miller, and K. Donaldson

Institute of Occupational Medicine, Edinburgh, Scotland

A mathematical model describing the dissolution and disintegration of long fibers and the clearance of short fibers is developed. For short fiber clearance, the model is based on previous modeling of the retention and clearance of particles, and most model parameters are taken from that particulate model. In addition to modeling the disappearance of long fibers, the present study includes a quantitative measure of goodness of fit of the model to observed data. Data from chronic inhalation experiments with insulation glass wools (MMVF10 and MMVF11) and rockwool (MMVF21) were provided for this study. These data comprised lung burdens at 10 time points at each of 3 concentrations for each fiber in inhalation experiments lasting up to 104 wk. At the two higher concentrations, the model had to take into account the effects of lung burden on macrophage-mediated clearance. The modeling shows that the overload dependence appears remarkably similar to that for low-toxicity particles in that the critical volumetric lung burden is similar to that for low toxicity dust. The model describes overload as leading to alveolar sequestration of short fibers or particles, and the estimated rate of alveolar sequestration for MMVF10 was similar to that for particles, but the estimated rate was lower for the other two fibers. Two alternative hypotheses to describe the process of the disappearance of longer fibers were tested by assessing their effect on a quantitative measure of fit of model predictions to the lung-burden data. These tests indicated that (a) dissolution leading to disintegration of long fibers into shorter fibers gave a much better fit than the alternative assumption that dissolution would leave only nonfibrous residue and (b) the relative rates of disintegration of the fibers in the lung appear to be directly dependent on their rates of in vitro dissolution and their diameters.

In modeling complex biological processes, it is often possible to describe broad trends using simple regression or other statistical models. However, when it is desired to model the evolution of a process over time, and particularly when the status of the process at any time point influences its subsequent course, it is necessary to develop dynamic models based around differential equations. In either case, the model will be more plausible if based upon an understanding of the underlying biological mechanisms.

A model is a mathematical equation or system of equations that, given quantitative inputs, predicts certain outputs. It can have many numerical parameters, often describing rates or proportions. In dynamic modeling, these may either be obtained from the work of other investigators or be estimated

Received 27 June 2002; sent for revision 12 August 2002; accepted 18 November 2002.

We acknowledge support from the Joint European Medical Research Board (JEMRB), which provided both the finance for this work and the data from the inhalation experiments.

Address correspondence to Dr. Alan Jones, Institute of Occupational Medicine, Roxburgh Place, Edinburgh EH8 9SU, Scotland. E-mail: iom@iomhg.org.uk

by maximizing the fit of predictions to observed data. The latter route may also enable discrimination between alternative model formulations representing different biological hypotheses. However, it is often the case that the structure of the model is more complex than the observations that can be made, and it is rarely possible to estimate all model parameters from a single data set. A complex model can valuably bring together qualitative assumptions and quantitative factors from a variety of sources; however, sensitivity analyses are usually needed to investigate the sensitivity of the predicted outputs to these assumptions and to individual parameter values (Saltelli et al., 2000).

The toxicity of respirable mineral fibers is expected to be a function of the cumulative dose of fibers in the lung. The cumulative burden depends on the inhaled fibers' deposition in the lung, their subsequent clearance from and transport within the lung, and any dissolution or disintegration of fibers in the lung. With the increasing pressure to reduce animal experimentation, a model to predict the retained burden would have real utility.

Mathematical models have been widely used previously to describe the deposition, retention, and clearance of inhaled particles (Tran et al., 1999a, 1999b). The first of previous studies at the Institute of Medicine (IOM) (Middleton et al., 1977, 1979) addressed differences in the deposition and clearance of different varieties of asbestos fibers following a 6-wk period of exposure. This was followed by an assessment of the effects of lung burden on the clearance of fibers (Bolton et al., 1983). Subsequent studies developed models to describe the deposition, clearance, and sequestration of fibers during chronic exposure, with data from animal studies with rats exposed for up to 1 yr using both fibers and other nonfibrous mineral dusts (Vincent et al., 1985, 1987; Jones et al., 1988, 1989). The consequences of the differences in the clearance (or durability) of amphibole and chrysotile asbestos have been examined in a relatively straightforward model of clearance (Jones et al., 1994).

More recently, we have extended these models to include descriptions of the cellular mechanisms involved in the clearance of particulate dusts from the lung (Tran et al., 1999a, 1999b, 2000), building upon the mechanistic models developed by Katsnelson (Katsnelson et al., 1992) for quartz and titanium dioxide particles, and by Stöber for particulate dust (Stöber et al., 1989, 1990). We now describe further extensions, to describe the behavior of fibers. These require additional fiber-specific model components, particularly in relation to changes to the fibers in vivo. Yu et al. (1994a, 1995) have also developed a model that describes the retention, clearance, dissolution, and disintegration of fibers and applied it to RCF1. Yu et al. (1997) modeled the clearance of manmade vitreous fibers (MMVF) after inhalation exposure for 5 days. Some of the results of that modeling were then used by Yu et al. (1998) to model the accumulation of fibers during ongoing exposure. Briefly, there were several common points with the work we describe here, and some areas of difference. For example, they used fiber lung-burden data from the same source, some but not all of the data that we used, and some data from a

different set of experiments. In particular, our modeling includes postexposure data that were not modeled by Yu et al.; our model is an extension of a clearance model that was developed for nonfibrous dust with many parameter values assigned from the modeling of particulate clearance. We examine the points of similarity and difference more closely in the discussion.

Although recent studies (e.g., Miller et al., 1999) suggest that the number of long (say >15 or >20 μm) fibers is one of the main factors in the risk of cancer in animals, fibers of shorter lengths may still be important. For example, most experimental studies on mesothelioma induction rely on injection of fibers directly into either the pleural or peritoneal cavity. However, the available evidence indicates that after inhalation, only shorter fibers reach the pleural lining and thus make direct contact with the mesothelial cells (Gelzleichter et al., 1999). While this direct contact may facilitate any involvement of short fibers in mesothelioma, it does not necessarily mean that the risk of mesothelioma arises solely from short fibers. Although they were looking for an association between fiber transfer to the pleura and development of pleural inflammation and fibrosis, Gelzleichter et al. (1999) noted that cytokine release from alveolar macrophages may mediate the proliferation of mesothelial cells.

In toxicology studies to assess relative risks, rats are exposed at high concentrations to balance the ethical requirement to use no more animals than necessary and the practical constraint of producing a response within the 2- to 3-yr life span of rats. Studies at these concentrations often produce lung burdens that overload the macrophage-mediated clearance mainly with short fibers. Therefore, a model of the kinetics of lung burden within such experiments needs to take account of overload. Thus, there are good reasons to address the retention and clearance of fibers of all lengths.

AIMS

The aim of the work described here was to develop a biologically based mathematical model of how the lung deals with inhaled fibers and to fit this model to available animal inhalation data for three fiber types (MMVF10, MMVF11, and MMVF21) in order to:

1. Assess whether the relative magnitudes of disappearance rates for long fibers, estimated from in vivo experiments, can be predicted from the relative sizes of the corresponding in vitro dissolution rates.
2. Assess the evidence that disintegration of long fibers (i.e., their breakage into two or more smaller fibers) is an important component of the process by which long fibers disappear from the lung.

METHODS

Data

Data were available from chronic inhalation studies (described by Hesterberg et al., 1993) conducted at the Research and Consultancy Com-

pany (RCC) with MMVF10, MMVF11 (glass insulation fibers), and MMVF21 (rockwool). In those experiments, rats were exposed to each fiber type for up to 104 wk at 3 levels of concentration: low (3 mg m^{-3}), mid (16 mg m^{-3}), and high (30 mg m^{-3}). Groups of rats were taken from exposure at intervals (13, 26, 52, 78, or 104 wk). For the first 4 groups, half of each group was killed immediately after removal from exposure and the remainder at 104 wk after start of exposure; for the group with 104 wk of exposure, half were killed at end of exposure and half 16 wk later. Thus there were 10 subgroups per concentration.

The amount of fiber in each rat lung was measured by digesting the accessory lobes of the lungs, then recovering the fibers for counting and sizing by scanning electron microscopy. Each subgroup normally contained 5 rats and the data consisted of measurements on 100 fibers per rat, for a total of about 500 fibers measured for the subgroup.

The data comprised:

- Aerosol fiber number concentrations.
- The lung (accessory lobe) burdens in total number of fibers for each animal.
- Bivariate (length and diameter) distributions for the aerosol and the fibers from the lungs.

To obtain sufficient numbers of measurements, size distributions were pooled across animals within each subgroup.

Model

Compartments of the model for the translocation of fibers in the lung
The starting point for our model is our previous model for the behavior of particles in the lung, with a shift in units from mass burden to fiber number burden. Figure 1 shows the locations within the lung and lymph node that form the nine spatial compartments of that model, X_1 to X_9, along with the routes of translocation between them. The locations are:

1. At the alveolar level.
   - Free (unphagocytosed) fibers deposited at the alveolar surface (X_1).
   - Fibers successfully phagocytosed by active alveolar macrophages (AMs) (X_2).
   - Fibers inside inactive alveolar macrophages which upon necrosis of these macrophages will be released back onto the alveolar surface for rephagocytosis (X_3).
   - Fibers sequestered in the alveolar sequestration compartment, i.e., fibers held in overloaded, immobile macrophages (X_4).

2. At the interstitial level.
   - Free (unphagocytosed) fibers in the interstitium (X_5).
   - Fibers successfully phagocytosed by interstitial macrophages (IMs) (X_6).

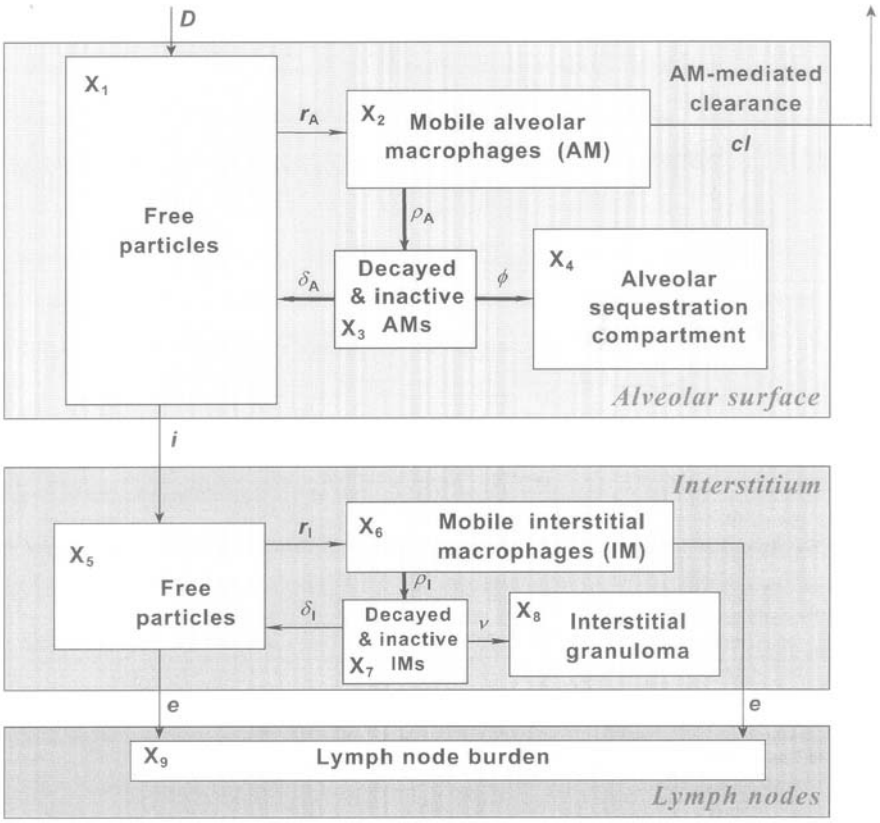

FIGURE 1. Scheme of the main translocation routes for short fibers, including the alveolar macrophage-mediated clearance, with the translocation routes labeled with the appropriate rate constant. See text for restrictions on the translocation and locations of long fibers.

- Fibers attached to inactive interstitial macrophages, which will be released back into the alveolar surface for rephagocytosis (X_7).
- Fibers sequestered in interstitial granuloma (X_8).

3. At the lymphatic level.
   - Fibers removed to the lymph nodes (X_9).

Mathematically, the translocation between the various compartments just described (along the arrowed routes) is represented by a set of differential equations, and these have been described previously for particles (Tran et al., 1999a, 1999b).

Subdivision of compartments by fiber length category The extension of the model to describe the behavior of fibers in the lung needs to reflect the beliefs that fiber dimensions would affect the ability of macrophages to phagocytose and remove fibers, and that the fibers themselves might undergo physical changes while in the lung, either by dissolution or by breakage,

or both. The compartments were therefore subdivided to represent the behavior of nine 5-μm categories to accommodate fibers up to 45-μm long. Thus the time-dependent outputs of the model were to be X_{ij}, representing the burden of fibers in the jth size category in compartment i.

Complete specification of the model then required translocation parameters as in Figure 1, some or all of which could differ by length category, and, if required, further parameters describing the rate(s) at which fibers moved between length categories.

Differences in translocation parameters by fiber length category The principal mechanism for movement of fibers between the location compartments of Figure 1 is by phagocytosis by AMs and IMs. Fibers with length as large or larger than the diameter of the alveolar macrophage are not always successfully phagocytosed by AMs (Oberdörster, 1994). Unsuccessful or frustrated phagocytosis hinders the macrophage motility, and hence impairs AM-mediated clearance. Partial phagocytosis would also be expected to hinder the interstitialization of the fiber. Further, long fibers are not efficiently transported to the lymphatics because of their size (Oberdörster et al., 1988). Since the average macrophage diameter is approximately 15 μm, we have assumed that short fibers ($l \leqslant 15$ μm) can be phagocytosed and transported among all the compartments similarly to particles. For the longest fibers, on the other hand, we propose a critical length l_{crit}, above which fibers are assumed to be too long to be cleared by macrophages and for which phagocytosis is unsuccessful. These long fibers can be removed only by mechanisms other than macrophage-mediated clearance, such as dissolution and/or disintegration. (Inspection of the data suggests l_{crit} to be between 20 and 25 μm, and we have used 20 as a cutpoint.) Long fibers will not reach compartments for alveolar sequestration, interstitial granuloma, or the lymph nodes, so the transfer parameters here were set to zero. Finally, for intermediate-length fibers ($15\ \mu m < l \leqslant l_{crit}$), it is assumed that successful phagocytosis occurs but more slowly than for short fibers, so lower values were used for these parameters.

Effect of fiber dissolution on disappearance To describe the effect of fiber dissolution on disappearance, a working definition of fiber dissolution must be stated explicitly: *The dissolution of fibers manifests itself in a reduction in diameter of the fibers in the lung*. By this definition, dissolution is different from leaching, in which fibers lose component elements without a change in fiber diameter.

The definition of dissolution just given is based on experimental in vitro data that show that glass fibers dissolve and the rate of reduction of the fiber's mass M is directly proportional to the fiber surface area S, that is,

$$\frac{dM}{dt} = k_{diss} S \tag{1}$$

where k_{diss} is the "dissolution rate" (in units of mass per unit surface area per unit time).

If the fibers are assumed to be cylinders with diameter D that decreases as dissolution proceeds, and the surface area of the ends is neglected, Eq. (1) can be solved to give (Eastes & Hadley, 1995):

$$D = D_0 - 2k_{\text{diss}} \frac{t}{\phi} \tag{2}$$

where ϕ is the density of this particular type of fiber and k_{diss} is the dissolution rate (ng m^{-2} h^{-1}).

Let D_m be the mean diameter of fibers in the diameter category m. Then the time taken for a fiber of diameter D_m to dissolve to D_{m-1} is:

$$t_{mk} = \frac{\phi(D_m - D_{m-1})}{2k_{\text{diss}}} \tag{3}$$

then

$$d_{mk} = \frac{1}{t_{mk}} \tag{4}$$

where d_{mk} (day^{-1}) is the transfer rate of fibers in length category k from diameter category m to diameter category $m - 1$.

If fibers break only after considerable dissolution, and obviously disintegration cannot occur after complete dissolution has taken place, then an initial estimate of the disappearance/disintegration rate (b_k) of fibers of length category k is:

$$b_k \approx d_{pk}$$

where p is the peak diameter category, i.e., the diameter category with the highest number of fibers, and d_{pk} is the transfer rate of fibers from the peak category to the category with zero diameter.

The effect of the disintegration of fibers on the numbers in different length categories is illustrated in Figure 2. The breakage of a fiber is assumed to produce two daughter fibers of half the length of the original. This model of size change is consistent with conserving the total length of fiber; for example fibers in the length range 30 to 40 μm become two daughter fibers in the length range 15 to 20 μm. The representation of each fiber producing two fibers of approximately half the length is a useful simplification, but a similar net output of daughter fibers might well have been obtained if we had used a more variable or complex pattern of size of daughter fibers. The equations allow each length category its own breakage rate (b_9 to b_1), but in practice the same value was used for b_3 to b_1 ($b_2 = b_1$) and $b_1 = 0$.

We can generalize the description of disintegration as the disappearance of long fibers and the corresponding creation of daughter short fibers, by

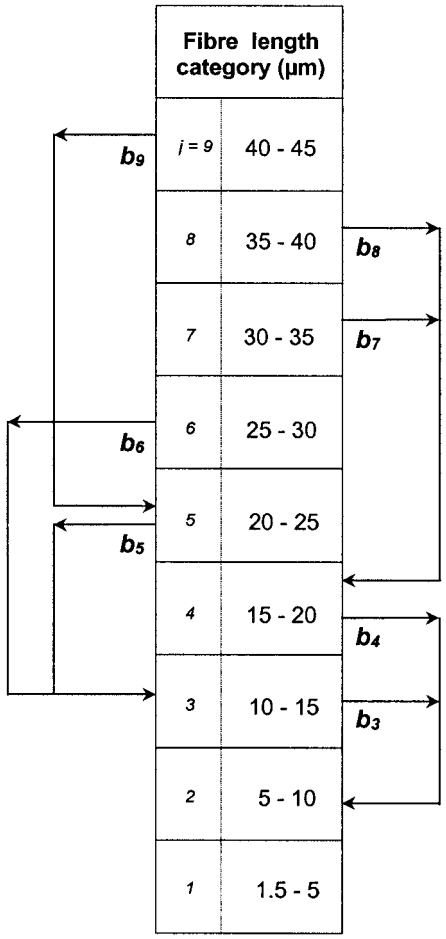

FIGURE 2. The second part of the model describing the breakage of fibers. Fiber disintegration takes place while fibers are located in the compartments described in Figure 1.

supposing that n is the number of short fiber fragments created from each disintegrating long fiber. An alternative hypothesis is that dissolution can be seen as the disappearance of a long fiber yielding no shorter fibers, i.e., $n = 0$. The alternative hypothesis of dissolution without breakage, i.e., $n = 0$, was also modeled and compared with the breakage model.

The complete model The complete model for fibers combines the translocation between biological compartments and the transformation by dissolution (with or without fiber breakage). The differential equations describing the evolution of the model over time are shown in Appendix 1. The various rate parameters are defined in Table 1. There are also parameters to define the input of deposited fibers, and the critical limiting values such as the critical fiber length for phagocytosis or the estimated critical lung burden for overload; these parameters are defined in Table 2.

Deposition of inhaled fibers The deposition of fibers was calculated with the breathing rate of the rat estimated as 0.2 L min^{-1}, that being at the center of the published range of values from 0.1 to 0.33 (Morgan et al., 1977; Yu et al., 1994). The rats were exposed for 6 h/day, which equates to an inhaled volume of 0.072 m^3/day of exposure. As exposure was conducted for 5 days/wk, and with a minimum exposure period of 13 wk in this study, it was appropriate to treat the concentration as averaged over the week (by multiplying the value by 5/7), as done previously by Morrow (1988).

TABLE 1. Clearance-rate parameters (day^{-1}) of the mathematical model of the breakage, retention, and clearance of fibers in the lung

Parameters	Symbol	MMVF10	MMVF11	MMVF21	Basis for value
Kinetics in macrophages					
Successful phagocytosis rate by AMs and IMs	r_l	4.00	4.00	4.00	Ass. P
Reduced rate of phagocytosis rate by AMs and IMs for fiber 15–l_{crit} long	r_j	**0.4**	**0.4**	**0.8**	**Est**
AM-mediated clearance of fibers	cl_j	0.015	0.015	0.015	Ass. P
Transfer rate of fibers from active to inactive AMs	ρ_j	0.14	0.14	0.14	Ass. P
Release rate of fibers back to the alveolar surface for rephagocytosis	δ_j	0.036	0.036	0.036	Ass. P
Kinetics of fiber transfer					
Interstitialization rate of free fibers	i_j	0.03	0.03	0.03	Ass. P
Translocation rate of fibers to the lymph nodes	e_j	0.001	0.001	0.001	Ass. P/Est
Overload and sequestration					
Motility decay coefficient	β	0.01	0.01	0.01	Ass. P
Alveolar sequestration rate	ϕ_j	0.14	**0.0075**	**0.0075**	Ass. P/**Est**
Rate of formation of interstitial granuloma	v_j	0.14	0.14	0.14	Ass. P
Fiber disintegration					
Disintegration rate of unphagocytosed fibers in length category k	b_k	**0.016**	**0.0088**	**0.0081**	**Est**
Disintegration rate of phagocytosed fibers (related to dissolution at low pH)	b_{LPk}	**0**	**0**	**0.0081**	**Est**

Note. Subscript j means that the parameter refers to fibers in length category j. Bold font highlights values that depend on fiber type. The final column indicates whether the values are based on either assumption from the particulate model (Ass. P) or an estimate (Est) obtained by comparisons with the lung burden data for the fibers. The values for the disintegration rates are reevaluated in comparison with values derived from in vitro dissolution rates later in the article. See text on the results from the sensitivity analysis.

TABLE 2. Parameters for the input of inhaled fibers and critical values (for fiber length, daughter fibers, and lung overload)

Parameters	Symbol	MMVF10	MMVF11	MMVF21	Unit
Deposition					
Deposited dose	D_j	Inhaled volume × deposition fraction (see Figure 3 for deposition fraction)			fiber wk^{-1}
Kinetics of fibers					
Critical fiber length beyond which phagocytosis is unsuccessful	l_{crit}	25	20	20	μm
Number of fibers of length category *j* generated by the breakage of a fiber of length category *k*	n_{jk}	2	2	2	
Overload and sequestration					
Critical fiber volume	V_{crit}	78	63	67	nl
Time when the critical fiber volume is reached	t_{crit}, τ_{crit}	Derived from concentration and V_{crit}			wk

The aerosol fiber concentrations were controlled to set mass targets of 3, 16, and 30 mg m^{-3}, and the number concentrations were estimated from regular samples evaluated by SEM (Table 3). The aerosol average size distributions were used to estimate the number concentrations of fibers within given length interval for each fiber type at each concentration. Then by qualitative inspection of model predictions of mean lung burdens first for total number of fibers and then for fibers within each length interval, estimates of the deposition efficiency were produced for each fiber.

Solving the Equations

The solution of a system of simultaneous ordinary differential equations (ODE) consists of the values of the output parameters (here numbers of

TABLE 3. WHO fiber number concentrations (fibers ml^{-1}) in the aerosol exposure (Hesterberg et al., 1993)

Mass concentration (mg m^{-3})	MMVF10	MMVF11	MMVF21	Mean
3	29 (± 7)	41 (± 29)	34 (± 13)	35
16	145 (± 35)	153 (± 69)	150 (± 51)	149
30	232 (± 56)	246 (± 76)	243 (± 67)	240

Note. WHO fibers are defined as having length >5 μm, diameter <3 μm, and aspect ratio >3:1; fibers meeting these criteria are counted in routine measurements of workplace concentrations.

fibers) at various points in time after the starting point t_0. If the system is complex, it is unlikely that an analytic solution is possible, and the solution has to be numerical. For the present model the Runge–Kutta fifth-order method has been used, as implemented by MATLAB (routine ode45). This algorithm is effective for solving linear and nonlinear systems of ODEs, and can vary the step of time extrapolation so that, in a stable region of the state space, a large step can be taken, resulting in a significant reduction of computation time. In an unstable state space region the Runge–Kutta algorithm will reduce the size of the step, at the cost of some increase in computation time.

Parameter Estimation

The values for parameters of the model were selected according to the following two criteria:

1. Quoted from literature.
2. Estimated from the experimental data available in this study.

Parameters selected according to criterion (1) (e.g., the macrophage phagocytosis rate *r*) were kept constant throughout the model simulations. Parameters derived from the data were estimated by a qualitative, visual assessment of the closeness of the model predictions to the experimental data. In some cases, such as the deposition fraction for fibers of different length categories, a range of possible values was known from literature and limited the choice.

In a study on the retention and clearance of "low-toxicity" dusts (Tran et al., 2000b), we have used numerical methods including both nonlinear regression and numerical solution of ODE. Also, we improved those methods in a recent study on silica (Tran et al., 2001). However, they were not applied in the work reported here, mainly because the methods applied were thought sufficient, but also because caution must be exercised in the interpretation and the usage of the estimated parameters obtained by numerical methods. For example, it is possible to obtain model parameters that would fit the model well to the data, but would not necessarily be unique.

Furthermore, if all the model parameters were treated as unknowns to be determined by fitting to the data, the problem would be mathematically intractable. Consequently, it is not merely sensible but necessary to assign some of the parameter values based on other information, such as prior estimates from modeling the retention and clearance of particles. (Table 1 indicates which parameters were assigned values in this way.) Only selected parameters were estimated by comparisons with the fiber data.

We checked the robustness of the selected parameters by qualitatively calibrating to part of the data set (the lower concentration experiments), and then checking the fit with the remaining data (the high concentration experiment). Then we used a sensitivity analysis to examine whether alter-

native parameter values would fit as well or better than the qualitatively selected values.

Model Predictions for Comparison with Data

The data comprised estimates of number and size distributions for fibers recovered from the accessory lobes. These were scaled up, by a factor of 10 as the accessory lobe is a 10th of the whole lung by mass, thus giving an estimate of the total lung burden. The model predictions were calculated as the sum of numbers of fibers in model compartments X_1 to X_{15}.

Model parameters and fit to the lung burden data For each fiber type at each concentration, the data available were estimated lung burdens of fibers in specific size categories and in various combinations of duration of exposure and postexposure recovery time. The model was set up to provide predictions of fiber lung burden for each of these combinations. If i is the index for exposure and recovery scenarios and j distinguishes fiber length categories, the results are a set of observed lung burdens o_{ij} for comparison with the corresponding predicted values e_{ij}.

For given i and j, a direct measure of comparison is the difference between observed and predicted values, $o_{ij} - e_{ij}$. To summarize the fit of a single model formulation to the data across all the categories, we need to combine these over length categories and over times, in a way that standardizes for dependence of the amount of variation on the fiber burden. If the only source of variation in the observed values were from random variation in the distribution and counting of fibers, we might expect that variation to be have a variance proportional to that from a Poisson distribution. Thus, before combining differences over lengths and times, we have standardized them by an estimated standard deviation based on an overdispersed Poisson model of variation.

$$r_{ij} = \frac{(o_{ij} - e_{ij})}{\sqrt{\mathrm{Var}(o_{ij})}}$$

Then, as a summary statistic, we have calculated the mean squared standardized distance (mssd):

$$\mathrm{mssd} = \Sigma r_{ij}^2 / M$$

where M is the number of (i,j) cells contributing to the sum.

Sensitivity of model predictions to values of each parameter The sensitivity of the model to the value of each of its parameters was examined by producing predictions for a fixed (10%) increase in each of the parameters in turn. Lung burdens were calculated for fibers subdivided by length classes and at each time point for which the model had previously been compared with experimental data. These calculated lung burdens were produced for the

model with parameters for MMVF10, MMVF11, and MMVF21 at three concentrations. Then each new prediction (for the 10% increase in a parameter) was compared with the original prediction by calculating standardized distance measures (the natural log of the new prediction divided by the original prediction) at each time point and within each size category. Mean and mean squared standardized distance measures were obtained by averaging across times, concentrations, and lengths. These standardized distance measures are an indication of the model's sensitivity to the change in parameter value.

All model parameters except two were included in the sensitivity analysis. The number of fibers generated per disintegration had previously been shown to be an important parameter, but examination of a 10% change was not feasible without more extensive changes to the model program. The other excluded parameter was the critical length for successful phagocytosis, as that critical length was evaluated directly from the experimental data.

RESULTS

Values for the Parameters of the Model

Table 1 shows the clearance-rate parameters, and in the last column defines how the values were obtained. Several values were assumed to be the same as in previous modeling of particulate dusts, such as titanium dioxide, which are considered to be "low-toxicity" or "nuisance" dusts. For example, the rate parameters for the kinetics in macrophages are the same as for the particles, except for the one parameter that is unique to fibers—the reduced phagocytosis rate for fibers with length 15 to l_{crit}. Other parameters, as identified in the final column, were estimated by comparisons of model with lung burden data.

The parameters for the transfer of fibers (from the alveolar surface to the interstitium, or short fibers from the interstitium to the lymph nodes) were assumed to be the same as for particles. The transfer to lymph node rate was assumed to be of the same order as for low-toxicity particles.

The rate coefficient describing the decay of macrophage motility as a function of fiber burden was also taken as being the same for particles. The alveolar sequestration rate for the MMVF10 was found to be the same as that for particulate dust. Interestingly, substantially lower values were judged to give better match with the data for the other two fibers.

The rate coefficients for the disintegration of fibers were initially derived by qualitative trial and error with values of b_k derived initially from the in vitro dissolution properties of the fiber.

Table 2 shows the other parameters of the model, the parameters with units other than day^{-1}. These include l_{crit} (the length above which fibers were too long to be cleared by macrophages), and n_{jk} (the assumed number of short fibers produced from each disintegrating long fiber). Their values were estimated from the fiber lung burden data. For each fiber type, the value of the critical lung burden (V_{crit}) was taken as the lung burden at the time point

(t_{crit}) judged to correspond to the start of overload in the data for the mid-dose (16 mg m^{-3}). The same value was then used in modeling the high dose experiment. These estimates of V_{crit} are strikingly and sensibly similar to the value (100 nl) applicable to nontoxic, nonfibrous particles.

The deposition of fibers into the lung is determined by the aerodynamic diameter of the fibers (a function of primarily diameter, density, and then length) for sedimentation and impaction, and additionally by length for interception. So unless the fibers all had the same density and same bivariate size distribution, the deposition efficiency would not be the same function of the univariate length distribution for all fibers. However, if the aerosol size distributions were not affected by the concentration, then deposition efficiency should be the same function of fiber length for each fiber type. In Figure 3, our estimates of deposition fraction, for fibers by length class interval, show clear differences between the fiber types, but with very little dependence on concentration. The data points were estimated independently for each exposure concentration of each fiber type. The data points show, in most cases, almost the same value across concentrations for a given fiber type; the few concentration-associated differences are small enough to be readily attributed to the uncertainty in the data. By contrast, the differences between fiber types are much larger, with MMVF21 (cross symbols) having the highest deposition fraction and MMVF10 (filled symbols) having the lowest at all

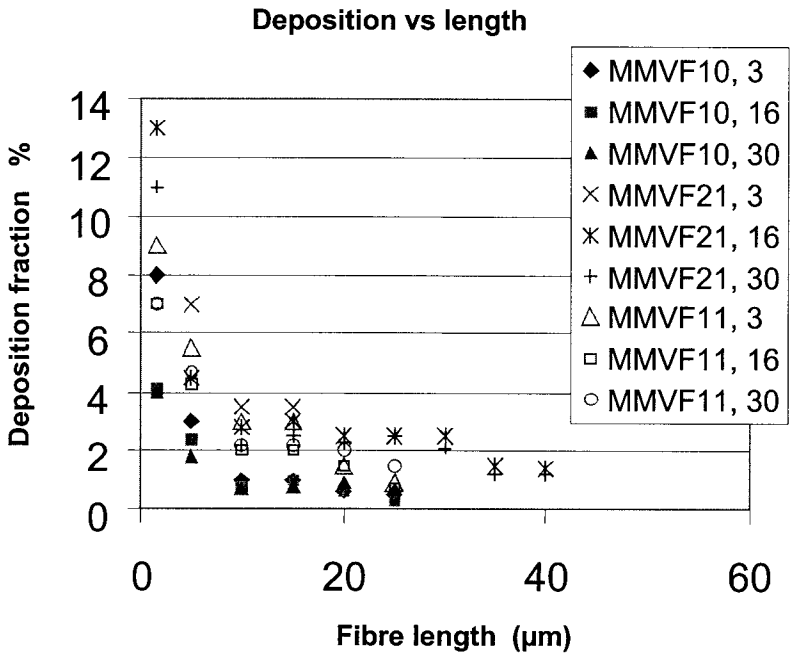

FIGURE 3. The deposition fraction estimated for fibers within length intervals (1.5–5, 5–10, 10–15, 15–20, 20–25, 25–30, 30–35, 35–40, and 40–45 µm), for each fiber type at three concentrations.

fiber lengths. Since deposition efficiency is primarily dependent on fiber diameter and density, and is approximately proportional to both, the higher deposition efficiency observed for MMVF21 means that MMVF21 has either a smaller mean diameter or lower density (or both) than the other fibers. However, MMVF21 actually has a higher density (2.79 g cm^{-3} compared to MMVF10 and MMVF11 at, respectively, 2.52 and 2.55 g cm^{-3}), so its mean diameter would have to be proportionately smaller again. Thus Figure 3 suggests that, for any given length of fiber, the mean diameter of MMVF21 was substantially smaller than that for MMVF10 and MMVF11.

Quantitative Tests of Alternative Hypotheses

In the comparisons of versions of the model with the lung-burden data, residuals were calculated for each subdivision of the data, i.e., the number of fibers in length intervals, at each exposure time point, and for three exposure concentrations. Residuals for particular subsets of the lung burden data were informative, but we focus on the overall performance as summarized by the mean square standardized distance (mssd) measures. For numerical convenience, these standardized measures were multiplied by 10^4.

Disappearance Rates

The mssd values were used to compare alternative estimates of the disappearance/disintegration rates for long fibers. For this purpose, the estimated rates of disappearance for long fibers, derived by qualitative comparisons of model and lung burden data, were used as a baseline against which to compare the alternatives.

Logically, we would expect that in vivo disappearance/disintegration rates (for the fibers on the alveolar surface) would be related to in vitro dissolution rates measured for fibers in a solution of neutral acidity (pH 7). Table 4 examines the possibility that the dissolution rate k_{dis} (in ng cm^{-2} h^{-1}) and the disappearance rate b_k (in day^{-1}) would be in the same proportion for the three fibers. Table 4 shows the mssd obtained when disintegration rates (b_k*) for MMVF11 and MMVF21 were calculated using the ratio of the estimate of b_k to the estimate of k_{dis} for MMVF10.

Dissolution at pH 4.5 is believed to be relevant to fibers in phagolysosomes in alveolar macrophages. The model includes disintegration of phagocytosed fibers, but it is assumed to affect only the fibers in the length range 15–20 μm. One size interval has relatively little influence on the mssd. So it is of relatively minor consequence (for mssd) to assume that the same proportionality would apply between in vitro dissolution at low pH and the disintegration rate for phagocytosed fibers b_{LPj}.

At the time of the model development, our information on the in vitro dissolution rates in low-pH liquid was only that for MMVF10 and MMVF11 the rate would be extremely low, and for MMVF21 the rate would be quite close to that for neutral pH. So, we had assumed b_{LPj} to be zero for MMVF10 and MMVF11 in the qualitative fitting of the model, and this is

TABLE 4. Model fit with the baseline model with empirically estimated disintegration rate b_k and with a revised model using in vivo disintegration rates derived from in vitro dissolution rates (from Zoitos et al., 2001) taking MMVF11 and MMVF21 to have the same proportionality as MMVF10 (i.e., 6×10^{-5})

	Baseline model, disappearance/ disintegration rates[a]			Model with disintegration rates derived from k_{dis}				
				In vitro dissolution rates for pH 7,[b] k_{dis} (ng cm^{-2} h^{-1})		Disappearance/ disintegration rates[c]		
Fiber	b_k (day^{-1})	b_{LPj} (day^{-1})	mssd	Mean	(Std dev)	b_k (day^{-1})	b_{LPj} (day^{-1})	mssd
MMVF10	0.016	0.001	21	259	(75)	Baseline model		21
MMVF11	0.010	0.001	34	142	(39)	0.0088	0.0006	33
MMVF21	0.008	0.008	11	23	(11)	0.0014	0.0031	25

[a] b_k estimated by inspection; b_{LPj} taken as nonzero for MMVF10 and MMVF11.
[b] From Zoitos et al. (2001); mean over 4 labs.
[c] Derived from in vitro dissolution rates (k_{dis}).

shown as zero in Table 1. However, the quantitative evaluation was undertaken later when there was more information, indicating small but nonzero rates for MMVF10 and MMVF11, and therefore these were the basis for the nonzero values for b_{LPj} in the baseline model as used to generate the mssd in column 4 of Table 4.

The mssd values in the final column of Table 4 are from the model with breakage rates assumed to be linearly proportional to the fiber's in vitro dissolution rate. These mssd values compare with those for the baseline model in the left-hand part of the table.

- For MMVF10, the model is unchanged, so no change in the mssd from column 4.
- For MMVF11, the mssd is marginally lower with b_k derived from the value of k_{dis} (33 compared to 34)—indicating the derived values (of b_{LPj} and/or b_k) to be as good, perhaps slightly better.
- For MMVF21, the mssd is higher with b_k derived from k_{dis} (25 compared to 11). This higher mssd is probably due to the difference in diameter of the MMVF21 fibers as compared to MMVF10 or MMVF11. Figure 2 (showing the deposition fraction for fibers of given length) indicated higher deposition for MMVF21, and that implies thinner diameter (and or lower density) for the MMVF21 fibers. This might well account for the breakage rate being relatively faster than would have been the case if k_{dis} had been the only difference between the MMVFs.

From the summary statistics in Table 4, it appears that the lung burden data support the supposition that the value of the in vivo disintegration rate is determined by the in vitro dissolution rate and by the diameter of the fibers in the lung. For MMVF11, a slightly improved fit is obtained by assuming linearity with the in vitro dissolution rate and ignoring the (probably slight) differ-

ence in diameter between MMVF10 and MMVF11 fibers of given length in the lung.

However, for MMVF21, the difference in diameter appears to be sufficiently large that the original empirical estimate of b_k gives a better fit than the assumption of constant proportionality without correction for the effect of fiber diameter.

Illustration of the Model Predictions for Long Fibers

Disappearance of long fibers Figures 4 and 5 illustrate how the model compares with the data.

The MMVF21 had fibers in more size intervals above 20 μm than had either of the other 2 fibers (which had negligible fibers longer than 30 μm), so we show the long fiber model for the MMVF21 in Figure 4. For this figure, we scale the data and model (multiplying both by the same factor) so that the model always reaches 1 at wk 104 for all 3 concentrations and for all fiber size intervals. For the plots of lung burden decreasing after cessation of exposure, the scaling is the same in principle (i.e., multiplication of both data and model by the same factor), but setting the start of the model curve to 100%. With this scaling, the model and data are compared with all three concentrations brought together within each graph. With the scaling, the model predictions from three concentrations very nearly collapse into a single curve, but there are slight differences (in the model for each concentration, e.g., with deposition rates). The slight differences in the scaled curves are perceptible only as slight thickening of the curve in Figure 4, but are more apparent (with two separate curves) in Figure 5b.

The data for the long fiber show that the pattern of lung burden changing with time, during and after exposure, is remarkably similar for the three concentrations (Figure 4).

Comparing the model with the data in the left-hand graphs of Figure 4, it appears that the model fits quite well with the data at the later three time points (52, 78, and 104 wk) during exposure. At the first two time points, the model appears slightly high compared to the data, as if the rate of disintegration is underestimated. In the right-hand graphs, it also appears that the rate of disintegration is slightly underestimated. However, the difference between model and data is small compared with the scatter typical of such lung-burden data.

Daughter fibers For the model, the disappearance of each long fiber was assumed to lead to the formation of two daughter fibers each having, on average, half the length of the parent fiber. An alternative premise was that each disappearance led to no daughter fibers. These alternatives were compared by calculating the mean square standardized distance measure (mssd) for n (the number of daughter fibers per breaking long fiber) at values of 2 and 0. The mssd was larger with $n = 0$ as compared to the values for $n = 2$:

- For each fiber at each concentration, by a factor ranging from 1.6 to 7.1.
- Over all comparisons, on average, by a factor of 3.6.

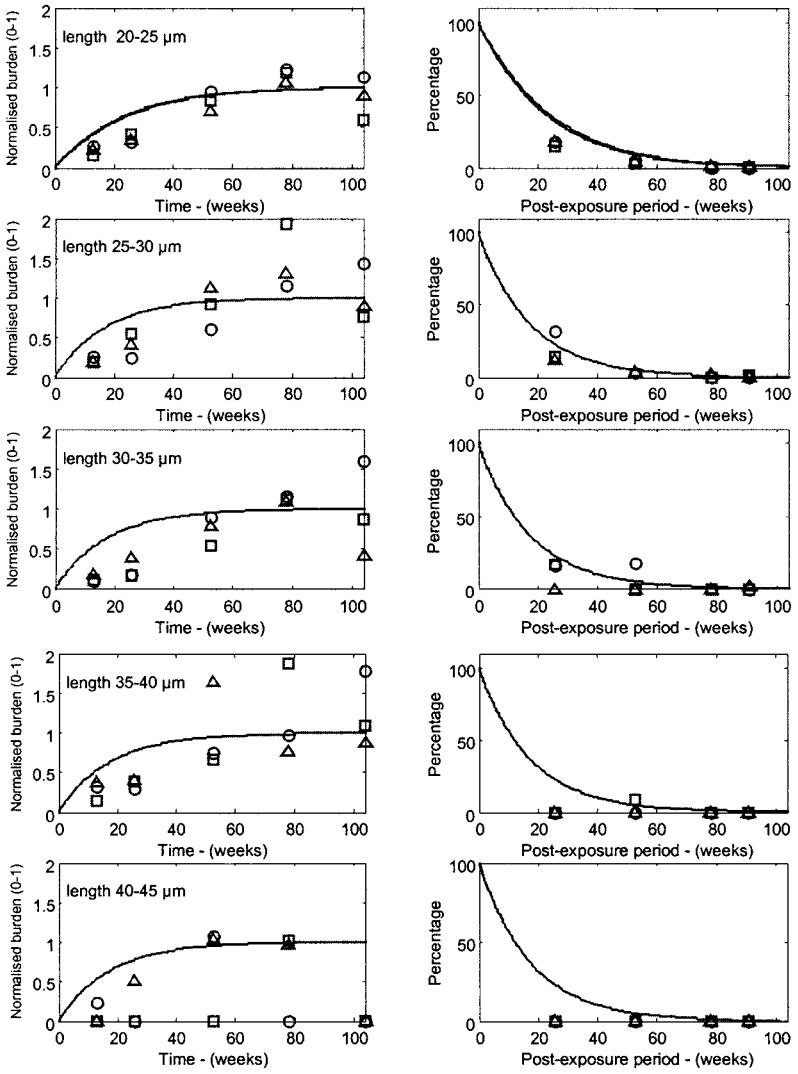

FIGURE 4. Kinetics of long fibers of MMVF21 at three concentrations. The postexposure clearance/disintegration graphs (right-hand graphs) show the retained lung burden as a percentage of the lung burden predicted at the end of each exposure period; this normalization was necessary as data came from a range of exposure periods and three concentrations. Correspondingly, the accumulation data and model were normalized such that the model reached 1 at 104 wk. (Disintegration parameters with values as in the baseline model of Table 4.) The symbols indicate the exposure concentration: ○ is 3 mg m^{-3}, □ 16 mg m^{-3} and Δ 30 mg m^{-3}.

So these tests supported the presumption that breakage of fibers would occur and so lead to formation of shorter fibers.

With a complex model, it is always worth considering whether certain alterations in the model predictions might be produced by changes in other parameters. However, in this case we think that is unlikely as the value of *n* has a very specific effect that is not duplicated by combinations of other

parameters. The result is good evidence of the formation of short fibers by fiber breakage.

Illustration of the Model Predictions for Short Fibers

The disintegration of the long fibers produces daughter fibers, and the model treats each disintegration as producing two daughter fibers with half

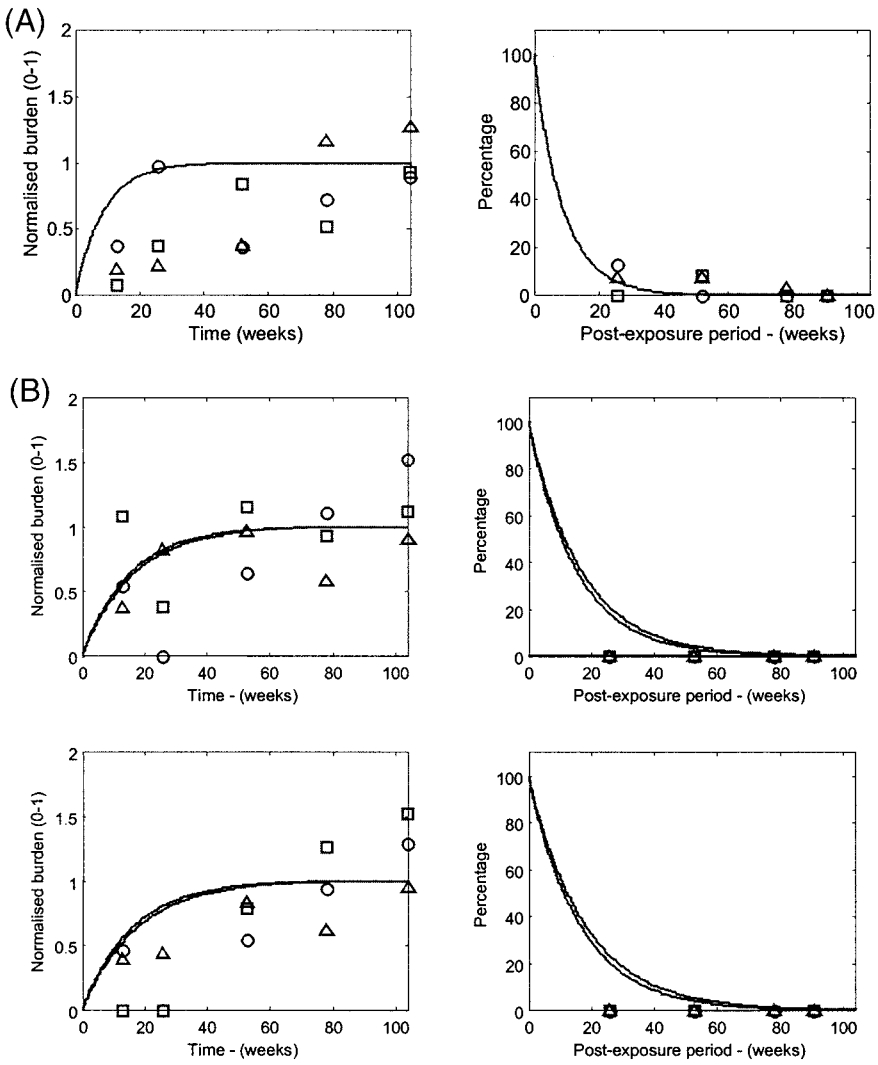

FIGURE 5. Kinetics of long fibers of MMVF10 (for one fiber length interval, 20–25 μm) and MMVF11 (for two length intervals, 20–25 and 25–30 μm). Each graph shows results for three concentrations: ○ is 3 mg m^{-3}, □ 16 mg m^{-3}, and Δ 30 mg m^{-3}. The model predictions (for the three concentrations) and data are normalized (by the same factor) such that the model predictions always reach 1 at wk 104, and postexposure disintegration starts at 100%. (A) MMVF10. (B) MMVF11 with disintegration rates derived from in vitro dissolution rate, as in Table 4, for fibers 20–25 μm long (upper graph) and 25–30 μm long (lower graph).

the length of the original fiber. These short fibers become part of the input of short fibers into the model of the clearance and retention kinetics for the short fibers. Given the differences in length distribution of the fibers, these inputs varied between the three fiber types.

At the lowest concentration, 3 mg m^{-3}, the lung burdens do not reach the volume that (for particulate dust) would be expected to cause overload. In the absence of overload, the model for retention/clearance is the same for the three fibers except that a rate of phagocytosis estimated for fibers in the intermediate length interval (15 to 20 μm) was lower for MMVF21 than for MMVF10 and MMVF11.

The plots of the short fiber results for MMVF21 are sufficient to demonstrate the main points; the results for the short fibers of MMVF10 and MMVF11 are in Appendix 2.

The plots in Figure 6 (for MMVF21) and in Appendix 1 (for MMVF10 and MMVF11) suggest that the model fits equally well for all three fiber types in the absence of overload (i.e., for exposure at 3 mg m^{-3}).

At the higher concentrations, the lung burdens reached the volumetric level at which impairment of macrophage-mediated clearance would be expected for a particulate dust. The model therefore includes overload. The data (Figure 7 for MMVF21, figures in Appendix 2 for MMVF10 and MMVF11) indicated that overload caused more retardation of clearance for the MMVF10 than for the other two fibers. Consequently, the alveolar sequestration rate (ϕ_l) needed two values to fit the model to the fiber data. Its value (0.14, see Table 1) for MMVF10 was the same as used previously for particulate dust. For the other two fibers, it had a lower value (0.0075) that was estimated from the data obtained at 16 mg m^{-3}; and this estimate was supported by the consistency of the model to the data at 30 mg m^{-3}.

At these higher concentrations, with the data showing a dependence on lung burden, the clearance curve was dependent on the duration of exposure. Given that the experiment was designed such that all postexposure lung burdens were measured at wk 104, the shorter clearance times correspond to longer exposure times and thus to the highest (i.e., slowest) clearance curve. So the data point at 26 wk postexposure corresponds to the slowest clearance curve in each of the graphs on the right (i.e., the uppermost curve). Similarly, the data point at 52 wk postexposure corresponds to the second slowest clearance curve.

Most Influential Parameters

Three parameters were identified as being the most important in the sense that a 10% change had the greatest impact on predicted lung burdens. These three were the rate of deposition (D), the rate of macrophage clearance (cl), and the disintegration rate (b_k) for fibers on the alveolar surface. The other model parameters all contribute to a lesser but nontrivial extent (although often the influence was restricted to certain length classes or certain time points). The effect on mean lung burden was largest for the

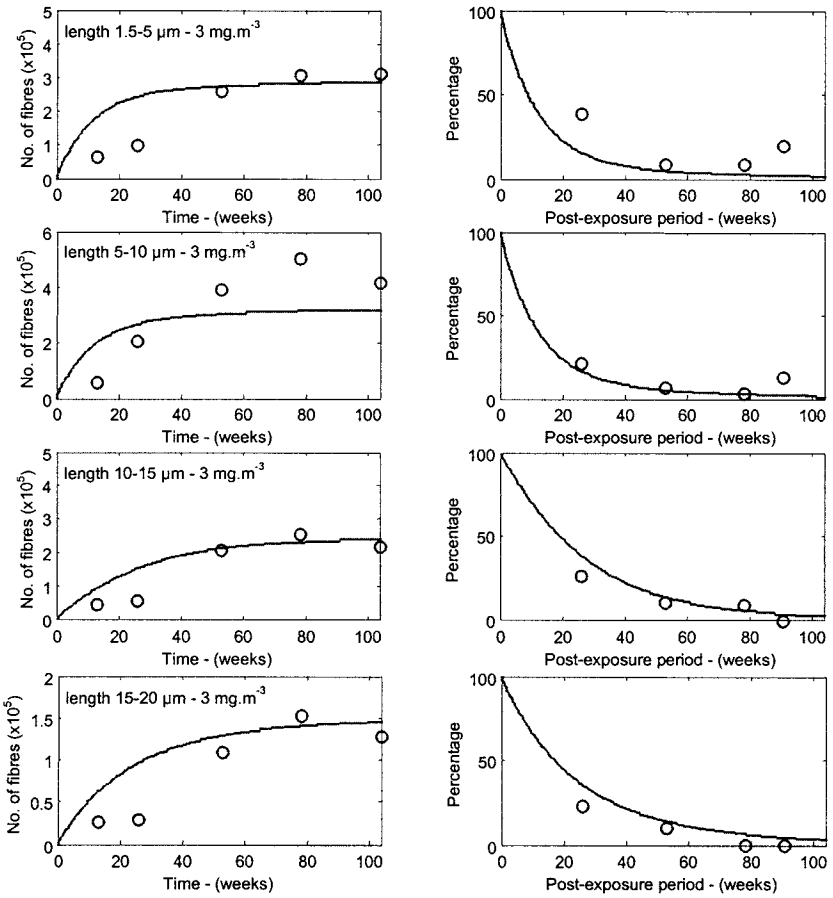

FIGURE 6. Kinetics of retention and clearance of short fibers at the low concentration (3 mg m^{-3}), described by the model without overload, for MMVF21.

deposition rate, and consistently for all 3 fibers, a 10% change in this parameter produced a 10% change in lung burden. However, the macrophage clearance rate and disintegration rate were less uniform across fibers; these 10% increments in cl and b_k had more effect for lung burdens of MMVF10 (at, respectively, 7% and 4%) and MMVF11 (8% and 4%) than for the MMVF21 (2% and 1%).

DISCUSSION

Development of Methodology

In this study we have proposed and used a biologically based mathematical model of the clearance and retention of inhaled fibers. The retention and clearance of short fibers is driven by the biological mechanisms of

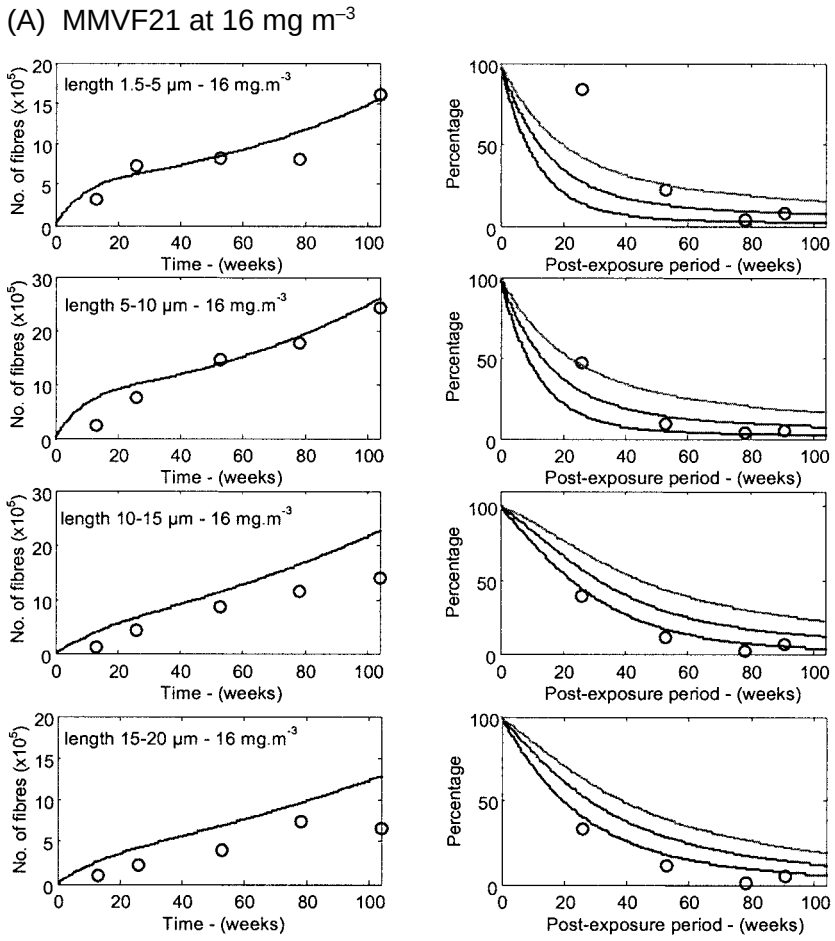

FIGURE 7. Kinetics of retention and clearance of short fibers at the two higher concentrations, described by the model with overload, for MMVF21: (A) MMVF21 at 16 mg m^{-3}. (B) MMVF21 at 30 mg m^{-3}.

macrophage-mediated clearance, transfer to the interstitium and lymph nodes—that is, the same mechanisms that are involved in the retention and clearance of particles deposited in the lung. For this part we have therefore been able to draw on existing models that have been shown to work well for dusts as various as TiO_2 and quartz (Tran et al., 1999a, 1999b; Tran & Buchanan, 2000), and have achieved an acceptable fit to short fibers also.

Fibers deposited in the deep lung differ from other particles in that some deposited fibers are too long to be cleared successfully by macrophages. Their disappearance from the lung is driven by the linked processes of dissolution and disintegration into shorter fibers. The mathematical modeling of these aspects with a direct linkage with this short-fiber model is a step forward that we hope will be useful in other contexts also. Although the present study has been concerned with three types of MMVF fiber, MMVF10,

MMVF11, and MMVF21, the model should be applicable to fibers generally.

Most of the model's parameters have been assigned values from previous modeling of particulate dusts, and in this study we have concentrated on the extensions: parameters pertaining to the disappearance of long fibers.

In the present study we have also developed and applied a quantitative summary measure of fit between model predictions and data. This serves to compare the fit for different model formulations, and to quantify how the fit for a particular formulation responds to changes in the parameters. Use of such measures is less subjective than the "by-eye" fitting that has served well in the past.

Dissolution and Disintegration of Fibers

We used the estimated disintegration rates for MMVF10 to calibrate a linear scaling from in vitro dissolution rates to in vivo disintegration rates.

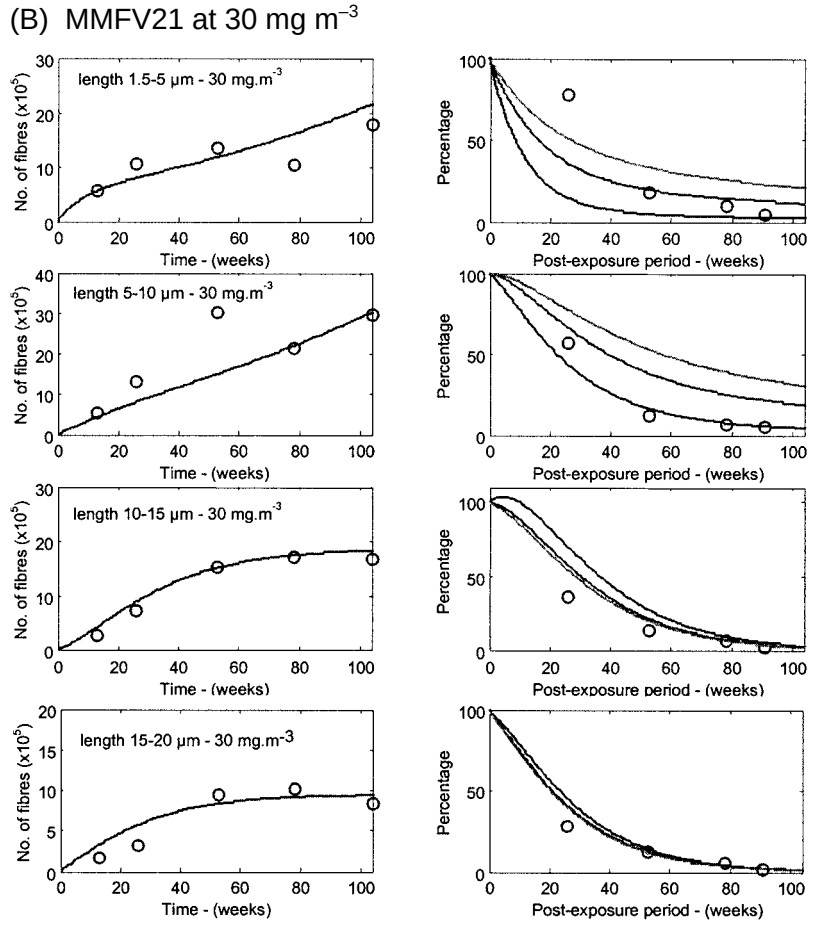

FIGURE 7. (*Continued*).

The linear scaling from in vitro values slightly improved the general model predictions (as compared to data) for MMVF11 fibers. For MMVF21 fibers, this scaling led to lower values of b_k and b_{LPj}, which gave predictions that did not fit as well as those obtained with their baseline values. However, in scaling dissolution rates from in vitro to in vivo, the fiber diameter was not taken into account. In modeling the deposition of MMVF21, we noted that long MMVF21 fibers had a higher deposition fraction than MMVF10 or MMVF11 fibers of the same length, suggesting that the MMVF21 were thinner and therefore would be expected to disintegrate more rapidly. So it is not surprising that, for MMVF21, a faster disintegration rate is better for describing the kinetics of the long fibers. The results suggest that if fibers have similar diameters, then the in vivo disintegration rates may be in direct proportion to the in vitro dissolution rates.

We also examined whether the kinetics of lung burden disappearance of fibers is better explained by pure dissolution (i.e., the continuous reduction in fiber diameter to nonfibrous residue) or dissolution driving disintegration into shorter fibers. We found that the disintegration model gave a very significantly better fit to the lung burden data for each MMVF. We modeled the process of disintegration as a continuous fragmentation of fibers (into two equal fragments) and found that this mode of disintegration gave a much better fit to the lung burden data for each MMVF. Although fragmentation is likely to produce nonequal fragments, our approximation produced plausible results when comparing to data.

Lung Burden of All Fibers

The high airborne concentrations used in toxicology studies on fibers and particles often overload and reduce the efficiency of the lung's clearance mechanisms. In our data, the overload effect appears very similar for fibers and nontoxic particles in that the critical volumetric lung burden is similar (about 100 nl) and the sequestration rate is either similar to (MMVF10) or lower than (MMVF11 and MMVF21) that for a well-tested low-toxicity dust (titanium dioxide).

The model of the disintegration of long fibers would be sufficient to calculate or predict lung burden for fibers longer than 20 μm. However, the overloading can contribute to inflammation and the development of fibrosis in long-term toxicity studies. The fibers shorter than 20 μm constitute the majority of fibers in the lung in tests with most fibers. If internal disintegration (inside macrophages) also occurs, then this can be an important part of the kinetics. So it is important to be able to predict the burden of fibers of all sizes, and the combined model is able to do that.

Consistency in Modeling

Our findings are broadly consistent with the studies by Yu et al. (1994a, 1995, 1997, 1998) on the retention and clearance of RCF and MMVF fibers, and with the study of Eastes and Hadley (1995) on the dissolution/disintegra-

tion of long fibers, in showing fiber dissolution to be the important mechanism in the removal of long fibers in the lung. We are also consistent with Yu et al. (1998) in finding that dissolution causes breakage into shorter fibers.

The modeling of Yu et al. (1997, 1998) used some data from experiments at RCC including some of the data that we have modeled here, i.e., the accumulation of lung burden during chronic exposure. We also used data from the postexposure phase of the experiments (the right-hand graphs in Figures 4 to 7). The main differences in the modeling approach were that we used more intervals of fiber size, with fiber length divided into intervals of 5 μm, whereas Yu et al. used 4 length intervals (<5, 5–10, 10–20, and >20 μm). Their assumed breakage pattern was somewhat different, which perhaps compensated for having fewer length intervals. They assumed that breakage rate increased with fiber length, whereas we found that a constant breakage rate sufficed. They had an equation that allowed their breakage rate to diminish with lung burden; however, their best fit constant for the parameter in the equation made the burden dependence very slight, which appears to support our assumption that breakage rate would be independent of burden. Both they and we correlated in vivo breakage rates with in vitro measurements of dissolution; they related the breakage rate to the log of the dissolution rate, whereas we found that a simple linear relationship sufficed. Given that the relationships are based on a limited number of fibers, and the breakage rates are applied to different assumed patterns of breakage, the main finding is that there is consistency in finding that the in vivo breakage rate increases with in vitro dissolution rate.

The Scope and Achievements of This Model

In this study, we have demonstrated that a single model, informed by understanding of the underlying biological processes, can predict lung burdens that agree with observed data for three types of MMVF across a range of exposure time and concentration. The model outputs agree reasonably well with the data for numbers of fibers in given length classes and for the mean lung burden as measured in subgroups of rats at 10 time points in each of 3 airborne fiber concentrations.

The model combines the previously described model (Tran et al., 1999a, 1999b) for the retention and clearance of particulate dust with a model of the disintegration of long fibers. The mechanism of disintegration would be expected to be unaffected by the lung burden; the data support this expectation and thus indicate the range for which disintegration is the main (or sole) mechanism of fiber disappearance at length greater than approximately 20 μm.

Comparison of the data with predictions from different model formulations supports the hypothesis that fiber disintegration, driven by dissolution, is likely to be the principal mechanism behind the disappearance of long fibers. The combination of deposition, clearance, dissolution, and disintegration controls the time-dependent lung burdens of fibers in various size

classes, which taken together will define a dose metric for the development of lung disease or damage. This in turn could provide a predictive tool for characterizing fibers with respect to their risk of causing respiratory disease.

APPENDIX 1: EQUATIONS OF THE MODEL

The model developed for particles was based on nine compartments defining the location of particles within the lung, and differential equations describing the rates of particle transport between these. Extension of the model to fibers needed to reflect that fibers of different length might be translocated at different rates, and that fiber dimensions might change through dissolution and/or breakage while in the lung. Thus the predicted fiber burdens at any time were indexed both by location and by length category, represented by X_{ij}, where the subscript i distinguishes the 9 compartments of physiological location shown in Figure 1 and j the 9 categories of fiber length in 5-μm categories up to 45 μm, as in Figure 2.

The transfer between the compartments is controlled by the transfer rates shown in Figure 1. Therefore the rate of change of fiber within each compartments is the sum of the transfer in (terms with positive sign) and the loss of fibers transferred from the compartment (terms with negative sign). Simultaneously, there is the transfer from one length category to another; fibers leave the length category due to breakage at rate b_j, while there is the addition of daughter fibers created by breakage of fibers longer than length j, i.e., from length categories with $k > j$ with n_k daughter fibers created from each breaking fiber in length category k. The inclusion of daughter fibers is expressed in the final term of Eqs. (A1) to (A8). In principle, the transfer rates and breakage rates may be assigned values specifically for each length category; however, in practice, this was limited to treating clearance as being progressively more affected if fibers were longer than 15 or 20 μm (see values of coefficients in Table 1).

The effect of "overload" retarding phagocytosis (r_j) and clearance (cl_j) was expressed by an overload function, which for these experiments with constant exposure concentration was expressed as a function (θ) of duration of exposure (t) [Eq. (A10)]. This overload function appears, moderating r_j and cl_j in Eqs. (A1) and (A2). The same function was also used to describe the concurrent increase in sequestration of fibers in alveolar granulomas or interstitial granulomas [Eqs. (A4), (A6), and (A7)]. It is also assumed to apply to describe the increasing rate of transfer to lymph nodes with overload [Eq. (A9), (A10)].

1. Free fibers on the alveolar surface (X_{ij}):

$$\frac{dX_{1j}}{dt} = D_j - \theta(t) r_j X_{1j} - b_j X_{1j} + \delta_j X_{3j} + \sum_{k>j} n_k b_k X_{1k} \qquad \text{(A1)}$$

2. Fibers inside AMs (X_{2j}):

$$\frac{dX_{2j}}{dt} = \theta(t)r_j X_{1j} - \theta(t)\mathrm{cl}_j X_{2j} - \rho_j X_{2j} - b_{\mathrm{LP}j}X_{2j} + \sum_{k>j} n_k b_{LPj}X_{2k} \quad \text{(A2)}$$

3. Fibers inside immobile/decayed AMs (X_{3j}):

$$\frac{dX_{3j}}{dt} = \rho_j X_{2j} - \theta(t)\delta_j X_{3j} - [1-\theta(t)]\phi_j X_{3j} - b_{\mathrm{LP}j}X_{3j} + \sum_{k>j} n_k b_{\mathrm{LP}k}X_{3k} \quad \text{(A3)}$$

4. Fibers inside alveolar granulomas (X_{4j}):

$$\frac{dX_{4j}}{dt} = [1-\theta(t)]\phi_j X_{3j} - b_{\mathrm{LP}j}X_{4j} + \sum_{k>j} n_k b_{\mathrm{LP}k}X_{4k} \quad \text{(A4)}$$

5. Free fibers in the interstitium (X_{5j}):

$$\frac{dX_{5j}}{dt} = i_j X_{1j} - r_j X_{5j} - e_j X_{5j} + \delta_j X_{7j} - b_j X_{5j} + \sum_{k>j} n_k b_k X_{5k} \quad \text{(A5)}$$

6. Fibers inside IMs (X_{6k}):

$$\frac{dX_{6j}}{dt} = \theta(t)r_j X_{5j} - \theta(t)e_j X_{6j} - \rho_j X_{6j} - b_{\mathrm{LP}j}X_{6j} + \sum_{k>j} n_k b_{\mathrm{LP}j}X_{6j} \quad \text{(A6)}$$

7. Fibers inside immobile/decayed IMs (X_{7j}):

$$\frac{dX_{7j}}{dt} = \rho_j X_{6j} - \theta(t)\delta_j X_{7j} - [1-\theta(t)]v_j X_{7j} - b_{\mathrm{LP}j}X_{6j} + \sum_{k>j} n_k b_{\mathrm{LP}k}X_{7k} \quad \text{(A7)}$$

8. Fibers inside interstitial granulomas (X_{8j}):

$$\frac{dX_{8j}}{dt} = [1-\theta(t)]v_j X_{7j} - b_{\mathrm{LP}j}X_{8j} + \sum_{k>j} n_k b_{\mathrm{LP}k}X_{8k} \quad \text{(A8)}$$

9. Fibers in lymph nodes (X_{9j}):

$$\frac{dX_{9j}}{dt} = e_j[\theta(t)X_{6j} + X_{5j}] \quad \text{(A9)}$$

where

$$\theta(t) = \begin{cases} 1 & \text{for } t \leq t_{\mathrm{crit}} \\ e^{-\beta(t-t_{\mathrm{crit}})} & \text{for } t > t_{\mathrm{crit}} \end{cases} \quad \text{(A10)}$$

(A1.1)

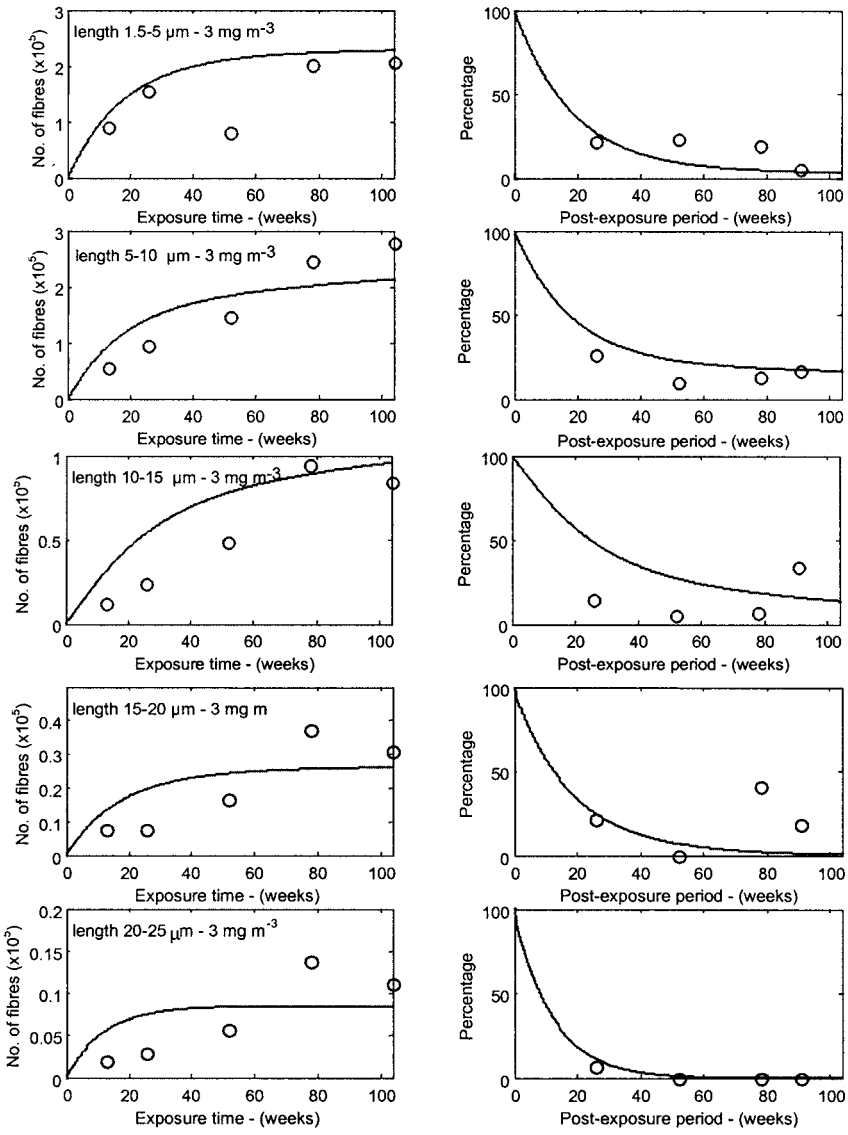

FIGURE A1. Kinetics of retention and clearance of short fibers at the low concentration, described by the model without overload: (A1.1) MMVF10 at 3 mg m^{-3}; (A1.2) MMVF11 at 3 mg m^{-3}.

(A1.2)

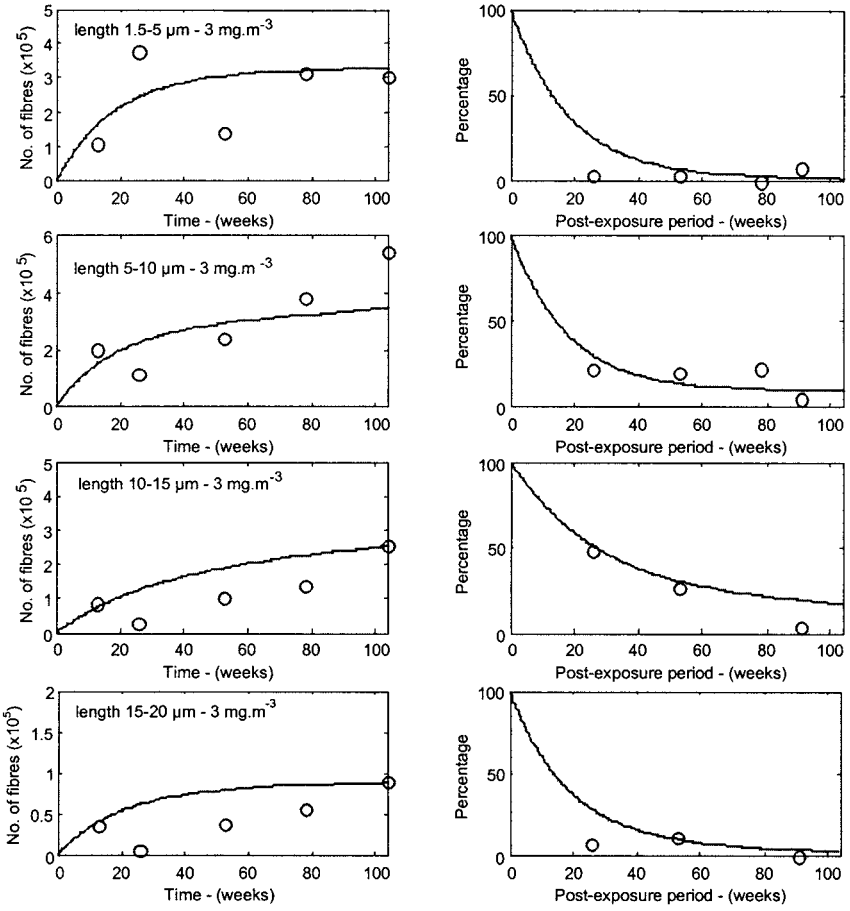

FIGURE A1. (*Continued*).

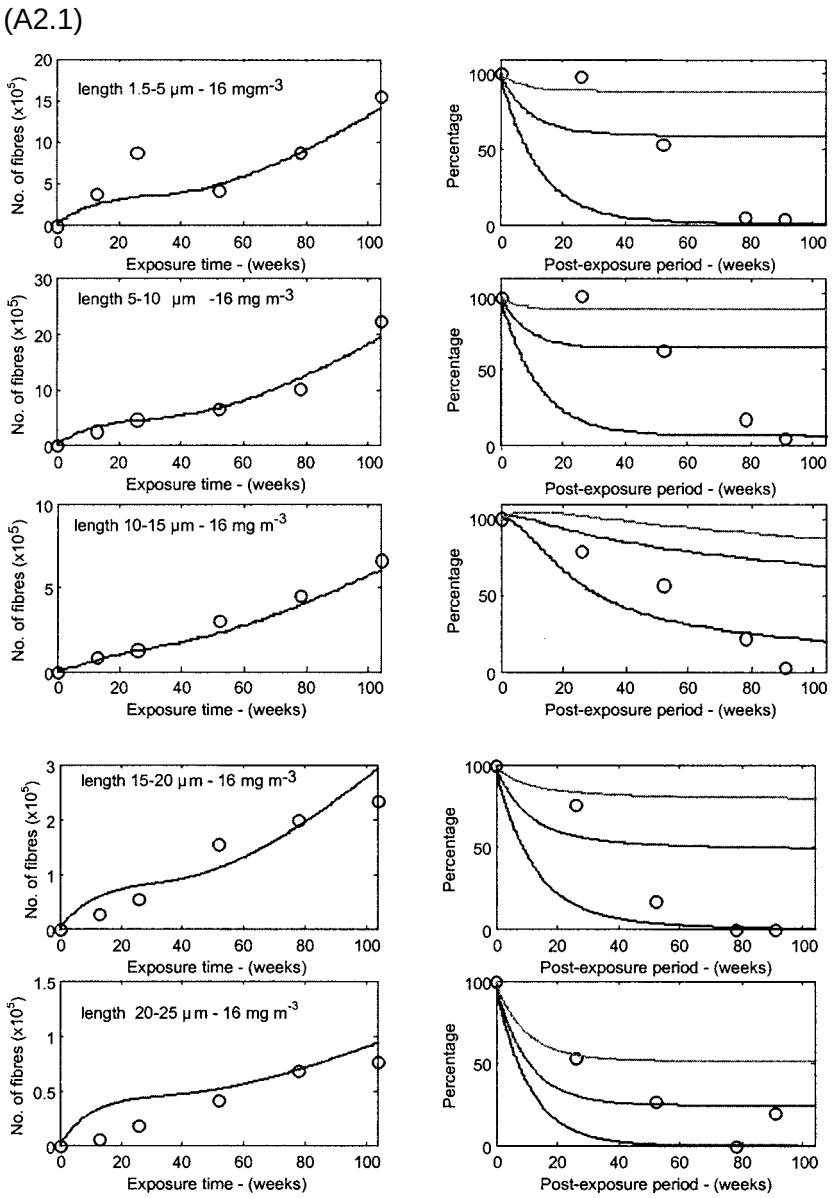

FIGURE A2. Fiber buildup during exposure (left) and corresponding clearance after exposure (right), at the two higher concentrations: (A2.1) MMVF11 at 16 mg m^{-3}, with three curves in each right-hand graph reflecting the effect of lung burden on clearance; top curve relates to the data point at 26 wk post-exposure (PE), from exposure for 78 wk; middle curve, data point at 52 wk PE from 52 wk of exposure; bottom curve, data points at 78 and 91 wk PE from 13 and 26 wk of exposure.

(A2.2)

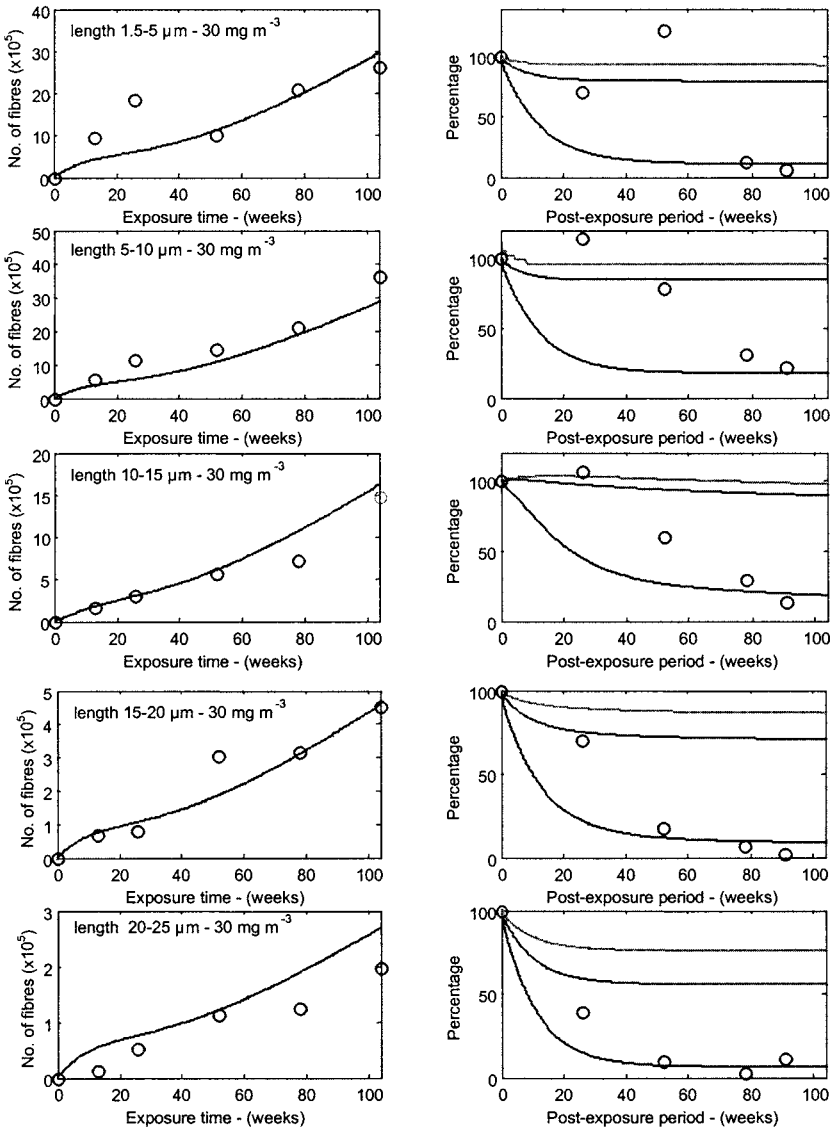

FIGURE A2. (*Continued*) (A2.2) MMVF10 at 30 mg m^{-3}, with three curves in each right-hand graph reflecting the effect of lung burden on clearance; top curve relates to the data point at 26 wk postexposure (PE), from exposure for 78 wk; middle curve, data point at 52 wk PE from 52 wk of exposure; bottom curve, data points at 78 and 91 wk PE from 13 and 26 wk of exposure.

(A2.3)

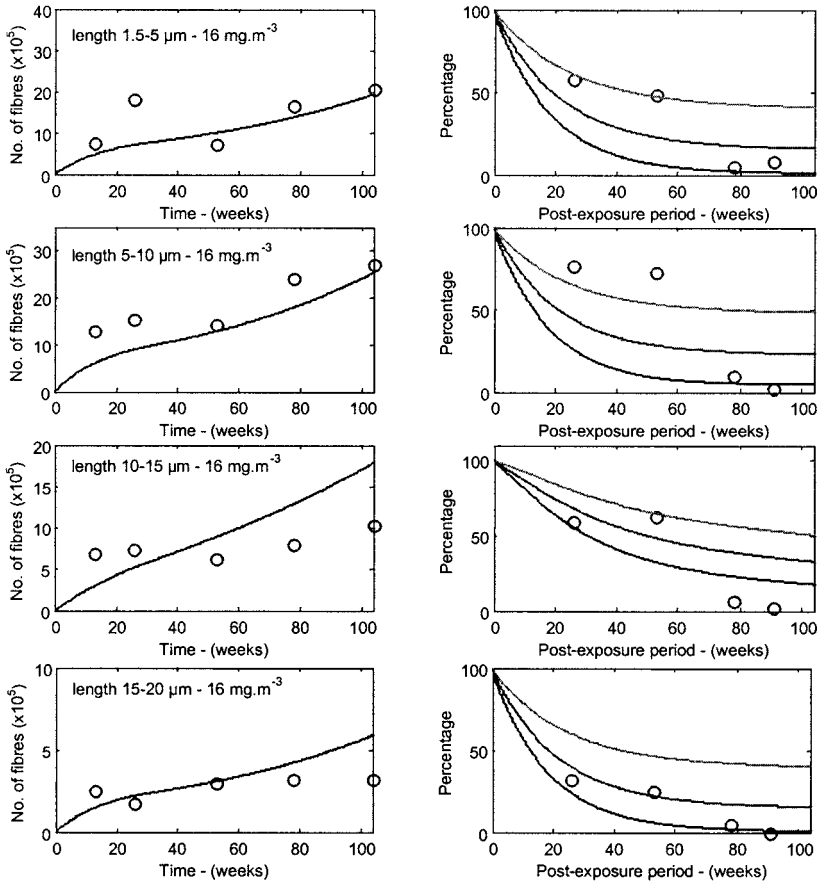

FIGURE A2. (*Continued*) (A2.3) MMVF11 at 16 mg m^{-3}, with three curves in each right-hand graph reflecting the effect of lung burden on clearance; top curve relates to the data point at 26 wk postexposure (PE), from exposure for 78 wk; middle curve, data point at 52 wk PE from 52 wk.

(A2.4)

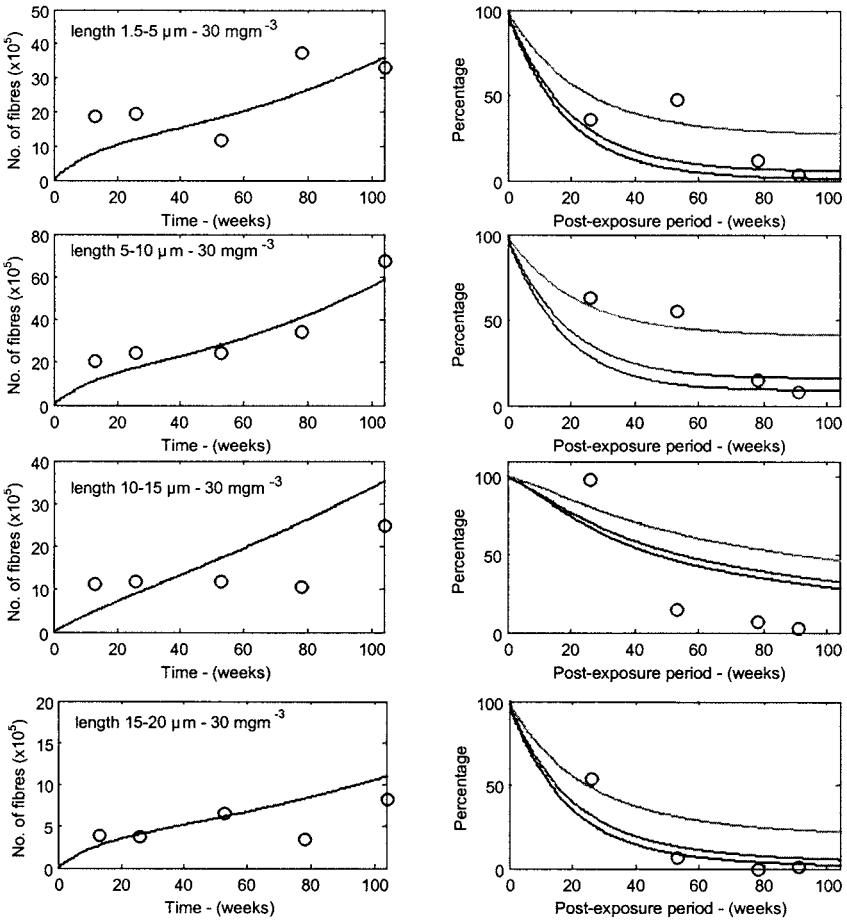

FIGURE A2. (*Continued*) (A2.4) MMVF11 at 30 mg m^{-3}, with three curves in each right-hand graph reflecting the effect of lung burden on clearance; top curve relates to the data point at 26 wk postexposure (PE), from exposure for 78 wk; middle curve, data point at 52 wk PE from 52 wk of exposure; bottom curve, data points at 78 and 91 wk PE from 13 and 26 wk of exposure.

REFERENCES

Bolton, R. E., Vincent, J. H., Jones, A. D., Addison, J., and Beckett, S. T. 1983. An overload hypothesis for pulmonary clearance of UICC amosite fibres inhaled by rats. *Br. J. Ind. Med.* 40:264–272.

Eastes, W., and Hadley, J. G. 1995. Dissolution of fibres inhaled by rats. *Inhal. Toxicol.* 7:179–196.

Gelzleichter, T. R., Bermudez, E., Mangum, J. B., Wong, B. A., Janszen, D. B., Moss, O. R., and Everitt, J. I. 1999. Comparison of pulmonary and pleural responses of rats and hamsters to inhaled refractory ceramic fibres. *Toxicol. Sci.* 49:93–101.

Hesterberg, T. W., Miller, W. C., McConnell, E. E., Chevalier, J., Hadley, J. G., Bernstein, D. M., Thevanaz, P., and Anderson, R. 1993. Chronic inhalation toxicity of size-separated glass fibers in Fischer-344 rats. *Fundam. Appl. Toxicol.* 20:464–476.

Jones, A. D., Vincent, J. H., McMillan, C. H., Johnston, A. M., Addison, J., McIntosh, C., Whittington, M. S., Cowie, H., Parker, I., Donaldson, K., and Bolton, R. E. 1988. *Animal studies to investigate the deposition and clearance of inhaled mineral dusts.* Final report on CEC Contract 7248/33/026. Edinburgh: Institute of Occupational Medicine. IOM Report TM/88/05.

Jones, A. D., Vincent, J. H., McIntosh, C., McMillan, C. H., and Addison, J. 1989. The effect of fibre durability on the hazard potential of inhaled chrysotile asbestos fibres. *Exp. Pathol.* 37:98–102.

Jones, A. D., Vincent, J. H., Addison, J., McIntosh, C., and Donaldson, K. 1994. Fate and effect of inhaled chrysotile asbestos fibres. In *Inhaled particles VII,* eds. J. Dodgson and R. I. McCallum, Proc. Int. Symp. on Inhaled Particles organized by the British Occupational Hygiene Society, Sept. 1991. Oxford: Elsevier Science. *Ann. Occup. Hyg.* 38(suppl. 1):619–629.

Katsnelson, B. A., Konysheva, L. K., Privalova, L. I., and Morosova, K. I. 1992. Development of a multicompartmental model of the kinetics of quartz dust in the pulmonary region of the lung during chronic inhalation exposure in rats. *Br. J. Ind. Med.* 49:172–181.

Middleton, A. P., Beckett, S. T., and Davis, J. M. G. 1977. A study of the short-term retention and clearance of inhaled asbestos by rats, using UICC standard reference samples. In *Inhaled particles IV,* ed. W. H. Walton, Proc. Int. Symp. Edinburgh, Sept. 1975. Vol. 1, pp. 247–258. Oxford: Pergamon Press.

Middleton, A. P., Beckett, S. T., and Davis, J. M. G. 1979. Further observations on the short-term retention and clearance of asbestos by rats, using UICC reference samples. *Ann. Occup. Hyg.* 22:141–152.

Miller, B. G., Jones, A. D., Searl, A., Buchanan, D., Cullen, R. T., Soutar, C. A., Davis, J. M. G., and Donaldson, K. 1999. Influence of characteristics of inhaled fibres on development of tumours in the rat lung. *Ann. Occup. Hyg.* 43:167–179.

Morgan, A., Evans, J. C., and Holmes, A. 1977. Deposition and clearance of inhaled fibrous minerals in the rat. Studies using radioactive tracer techniques. In *Inhaled particles IV*, ed. W. H. Walton, Proc. Int. Symp., Edinburgh, 1975, Vol. 1, pp. 259–272. Oxford: Pergamon Press.

Morrow, P. E. 1988. Possible mechanisms to explain dust overloading of the lungs. *Fundam. Appl. Toxicol.* 10:369–384.

Oberdörster, G. 1994. Macrophage-associated responses to chrysotile. *Ann. Occup. Hyg.* 38:601–615.

Oberdörster, G., Morrow, P. E., and Spurny, K. 1988. Size dependent lymphatic clearance of amosite fibres in the lung. *Ann. Occup. Hyg.* 32:149–156.

Saltelli, A., Chan, K., and Scott, E. M., eds. 2000. *Sensitivity analysis.* Chichester: John Wiley & Sons.

Stöber, W., Morrow, P. E., and Hoover, M. D. 1989. Compartmental modeling of the long-term retention of insoluble particles deposited in the alveolar region of the lung. *Fundam. Appl. Toxicol.* 13:823–842.

Stöber, W., Morrow, P. E., and Morawietz, G. 1990. Alveolar retention and clearance of insoluble particles in rats simulated by a new physiology-oriented compartmental kinetics model. *Fundam. Appl. Toxicol.* 15:329–349.

Tran, C. L., and Buchanan, D. 2000. *Development of a biomathematical lung model to describe the exposure–dose relationship for inhaled dust among U.K. coal miners.* Edinburgh: Institute of Occupational Medicine. IOM Report TM/00/02.

Tran, C. L., Jones, A. D., Cullen, R. T., and Donaldson, K. 1999a. Mathematical modeling of the retention and clearance of low-toxicity particles in the lung. *Inhal. Toxicol.* 11:1059–1076.

Tran, C. L., Jones, A. D., Cullen, R. T., and Donaldson, K. 1999b. Exploration of the mechanisms of retention and clearance of low-toxicity particles in the rat lung using a mathematical model. *Inhal. Toxicol.* 11:1077–1108.

Tran, C. L., Buchanan, D., Miller, B. G., Jones, A. D., and Donaldson, K. 2000a. Mathematical modeling to predict the responses to poorly soluble particles in rat lungs. *Inhal. Toxicol.* 12(suppl. 3): 403–409.

Tran, C. L., Graham, M. K., and Buchanan, D. 2001. *A biomathematical model for rodent and human lung describing exposure, dose, and response to inhaled silica*. Edinburgh: Institute of Occupational Medicine. IOM Report TM/01/04.

Vincent, J. H., Johnston, A. M., Jones, A. D., Bolton, R. E., and Addison, J. 1985. Kinetics of deposition and clearance of inhaled mineral dusts during chronic exposure. *Br. J. Ind. Med.* 42:707–715.

Vincent, J. H., Jones, A. D., Johnston, A. R., Bolton, R. E., and Cowie, H. 1987. Accumulation of inhaled mineral dust in the lung and associated lymph nodes: implications to exposure and dose in occupational lung disease. *Ann. Occup. Hyg.* 31:375–393.

Yu, C. P., Zhang, L., Oberdörster, G., Mast, R. W., Glass, L. R., and Utell, M. J. 1994a. Clearance of refractory ceramic fibres (RCF) from the rat lung: Development of a model. *Environ. Res.* 65:243–253.

Yu, C. P., Zhang, Z., Oberdörster, G., Mast, R. W., Glass, L. R., and Utell, M. J. 1994b. Deposition modelling of refractory ceramic fibers in the lung. *J. Aerosol Sci.* 25:407–417.

Yu, C. P., Ding, Y. J., Zhang, L., Oberdörster, G., Mast, R. W., Glass, L. R., and Utell, M. J. 1995. Deposition and clearance modeling of inhaled kaolin refractory ceramic fibers (RCF) in hamsters—Comparison between species. *Inhal. Toxicol.* 7:165–177.

Yu, C. P., Dai. Y. T., Boymel, P. M., Zoitos, B. K., Oberdörster, G., and Utell, M. J. 1998 A clearance model of man-made vitreous fibres (MMVFs) in the rat lung. *Inhal. Toxicol.* 10:253–274.

Yu, C. P., Dai. Y. T., and Ding, Y. J. 1998 A retention model of man-made vitreous fibres (MMVFs) inhaled by rats. *Aerosol Sci. Technol.* 29:152–162.

Zoitos, B. K., De-Meringo, A., Rouyer, E., Thélohan, S., Bauer, J., Law, B., Boymel, P. M., Olson, J. R., Christensen, V. R., Guldberg, M., Koenig, A. R., and Perander, M. 1997. In vitro measurement of fiber dissolution rate relevant to biopersistence at neutral pH: An interlaboratory round robin. *Inhal. Toxicol.* 9:525–540.